JOURNAL OF MATERIALS SCIENCE 33 (1998) 3985–3991

Oxyapatite in hydroxyapatite coatings

K.A. GROSS*
Department of Materials Engineering, Monash University, Clayton 3168, Australia

C.C. BERNDT
Department of Materials Science and Engineering, State University of New York at Stony Brook, Stony Brook, NY 11794-2275 USA

P. STEPHENS, R. DINNEBIER[1]
Department of Physics, State University of New York at Stony Brook, Stony Brook, NY 11794-3800, USA
E-mail: karlis.gross@eng.monash.edu.au

Plasma sprayed hydroxyapatite coatings are used as bioactive surfaces for increasing the fixation of bone to the dental implants or orthopaedic prostheses. The variability in the performance of these coatings is partly attributed to the chemical phases that form at high temperatures in the plasma or fast cooling rates upon deposition. Hydroxyapatite can be accompanied by an amorphous phase constituent, tricalcium phosphate, tetracalcium phosphate, calcium oxide or the rarely mentioned oxyapatite. The high temperatures in the plasma produces a hydroxyl-depleted layer on the outside of the traversing hydroxyapatite particle. It is this dehydroxylated area which may form oxyapatite upon deposition. Higher cooling rates produce an amorphous phase, but a lower cooling rate will lead to the formation of oxyapatite. Examination of the coating at various depths with X-ray diffraction reveals a higher oxyapatite content in the underlying layers. The surface in contact with water vapour in air can be modified by the inclusion of hydroxyl ions to form oxyhydroxyapatite or hydroxyapatite. This presence and varying amounts of oxyapatite with coating thickness could influence the dissolution and mechanical performance of the coating for dental and orthopaedic prostheses.

1. Introduction

Manufacture of hydroxyapatite implants for biomaterial applications by thermal processing involves ionic transport through the apatitic structure. The presence of the OH^- ions within the structure enables stoichiometric hydroxyapatite to be heated to temperatures as high as 1400 °C. Dehydration due to a lower partial pressure of water at higher temperatures [1] can, however, produce oxyhydroxyapatites and also lead to decomposition products of tricalcium phosphate and tetracalcium phosphate [2]. The control of the hydroxyl concentration has produced useful properties for applications such as humidity sensors [3], carbon dioxide gas sensors [4] or fuel cells [5]. The hydroxide content of the crystalline phase in hydroxyapatite coatings is also important for medical applications and will influence the performance of the coating.

The removal of structural water from the lattice of hydroxyapatite produces a solid solution of hydroxyapatite and oxyapatite or, alternatively, a combination of both hydroxyapatite and oxyapatite, depending on the heating and cooling conditions. Depleted hydroxyl levels have been measured by Fourier transform infrared spectroscopy [6, 7], Raman spectroscopy [7, 8], nuclear magnetic resonance [9] and thermal gravimetric analysis, [10]; however, it is not possible to differentiate between a solid solution and the individual components. This distinction is possible with X-ray diffraction which is sensitive to small changes in the lattice.

X-ray diffraction makes use of the larger *c*-axis dimension of oxyapatite [11, 12], which manifests itself as a shift in the (0 0 *l*)-type peak to smaller angles, enabling determination of the amount of oxyapatite and hydroxyapatite within coatings. Hydroxyapatite has two such peaks, (0 0 2) positioned at $2\theta = 26.1^\circ$ and (0 0 4) at 53.1° in X-ray diffraction patterns obtained with Cu Kα radiation. Oxyapatite is most easily seen with a (0 0 *l*)-oriented flame-sprayed hydroxyapatite coating at large angles (Fig. 1a). Detection in plasma-sprayed coatings with random crystal orientation is more difficult owing to the breadth of copper Kα radiation (Kα_1, 1.544 Å; Kα_2, 1.540 Å) and

*To whom all correspondence should be addressed.
[1] *Present address*: Laboratory of Crystallography University of Bayreuth, D-95440 Bayreuth Germany.

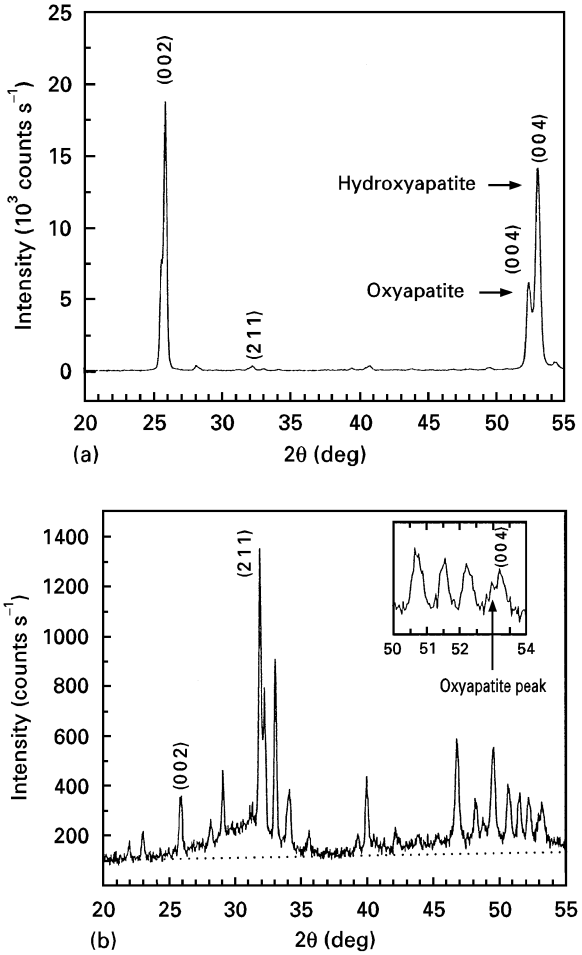

Figure 1 X-ray diffraction pattern of (a) a (00*l*) oriented flame-sprayed coating and (b) a plasma-sprayed hydroxyapatite coating. The inset of (b) indicates the spreading of the (004) peak by oxyapatite.

the broad diffraction peaks arising from fine grain size and residual stresses within the coatings (Fig. 1b). However, the distortion of the peak at 53.1° shown on the inset suggests a contribution from oxyapatite. X-ray diffraction patterns produced by other workers [13] have also shown a doublet at 53.1°. Decomposition products, such as β-$Ca_3(PO_4)_2$ or the titanium substrate have peaks in close proximity to the (004) peak and may mask the peak of interest (Table 1).

The purpose of this study is to examine oxyapatite with X-ray diffraction using a conventional X-ray source and synchrotron-generated radiation. A model will be proposed to explain its formation in plasma-sprayed coatings. Finally, the reactivity of this phase will be discussed by examining the change in the surface composition after spraying and probing to different coating depths. Phase transformations other than hydroxyapatite to the amorphous phase and oxyapatite are possible in plasma-sprayed hydroxyapatite [14–17] but will not be discussed in this paper.

2. Materials and methods

Hydroxyapatite was plasma sprayed using a Metco 3MB torch (Sulzer-Metco, Westbury, NY) with a GH nozzle. Argon and helium at 100 lbf in^{-2} were used as plasma gases and spraying was conducted at a power level of 25 kW. Hydroxyapatite powder was fed externally to the gun at a rate of 3.5 g min^{-1} with an argon carrier gas and the substrate held 12 cm away from the torch. The substrate was not cooled except where indicated. A coating was produced to a thickness of about 50 μm.

2.1. Conventional X-ray analysis

Coatings in the as-sprayed condition were analysed by conventional X-ray diffraction on a Phillips PW1729 (Eindhoven, The Netherlands) automated diffractometer using Cu Kα radiation. A step size of 0.01° with a collection time of 5 s at each angular increment was used to collect the angle and intensity data on the 1710 controller over a 2θ range of 20–60°. The tricalcium phosphate content present in coatings produced at low power levels is approximately the same for the different spraying conditions and is assumed to be the primary crystalline phase formed upon solidification close to the eutectic point [2]. According to the lever rule this quantity is approximately 5 wt% and therefore, it was not analysed quantitatively. The amorphous phase was quantitatively determined by comparing the ratio of the diffuse peak (centred at 31°) area to the crystalline peak area with known mixtures of amorphous and hydroxyapatite phases [10]. No distinction was made between the oxyapatite and the hydroxyapatite at this stage. The direct comparison method was used to calculate the amount of oxyapatite [18]. It was obtained by measuring the (004) peak area of oxyapatite and hydroxyapatite.

Table 1
Location of diffraction peaks positioned around the (004) peak of hydroxyapatite with the use of Cu Kα radiation

Compound	2θ (deg)	*d*-spacing (Å)	Reference card
Hydroxyapatite	53.1	1.722	Joint Committee of Powder Diffraction Standards, Card 9-432
Oxyapatite	52.6	1.740	Ref. [11]
β-$Ca_3(PO_4)_2$	52.9	1.728	Joint Committee of Powder Diffraction Standards, Card 9-169
Titanium	53	1.726	Joint Committee of Powder Diffraction Standards, Card 5-682

Since the apatites have the same structure and the peaks are positioned very close to each other, it can be assumed that the multiplicity factor and the temperature factor do not vary. This enables the area fraction of the peaks to be used as an approximation of the weight fraction of the two phases.

2.2. Synchrotron X-ray analysis

The use of X-rays of different wavelengths permits the determination of depth profiles [19]. Here, we used that capability to estimate the epth of dehydroxylation within the coating. Besides the adjustable wavelength, synchrotron radiation powder X-ray diffractometry generally offers higher intensity and resolution than conventional laboratory instruments. X-rays from beamline X3B1 at The National Synchrotron Light Source, Brookhaven National Laboratory, were selected by a Si(1 1 1) double crystal monochromator before the sample, and diffracted from a Ge(1 1 1) analyzer before the NaI scintillation detector. This configuration of parallel X-ray beams does not defocus if the incident and diffracted angles from the sample are unequal, and so psi scans would have remained sharp. However, in the present case it was more advantageous to minimize the influence of sample texture, and so the depth profile information was obtained by using different wavelengths in a theta-2theta diffraction geometry. The depth sampled depends both on wavelength and diffraction angle, and so the penetration (1/e) depth of X-rays into hydroxyapatite of nominal density has been computed and plotted in Fig. 2. The wave vector Q (defined as 4 pi sin(theta)/lambda) is equal to $2\,\mathrm{pi}/d$, where d is the spacing between diffracting planes. At low X-ray energies the penetration does not differ significantly as a function of incident angle but, at higher X-ray energies, composition information can be obtained from two different depths from the same X-ray diffraction patterns.

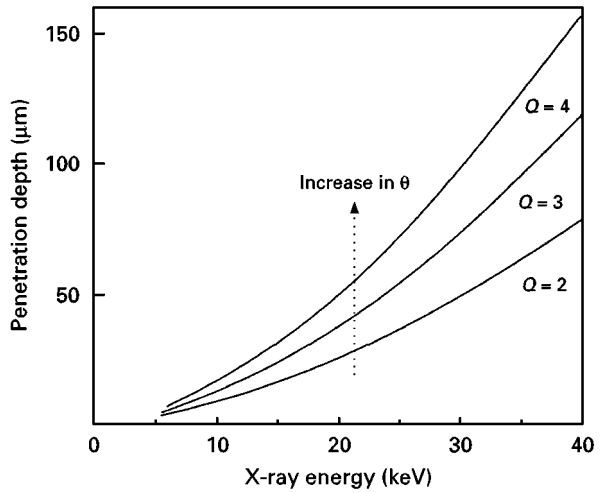

Figure 2 Penetration of the X-ray beam with a change in wavelength for hydroxyapatite. Q represents the scattering vector where $Q = (4\pi \sin\theta)/\lambda$. For a fixed X-ray energy, a larger incident angle produces a larger value of Q and a corresponding increase in X-ray penetration or sampling depth.

The position of a given peak is dependent upon the wavelength of the radiation and so the scan range was sifted to lower angles when a larger X-ray energy (shorter wavelength) was used. The most intense hydroxyapatite peak, the (2 1 1) found at 31.8 degrees of Cu K alpha (Q = 2.23), was used to normalize all of the patterns.

3. Results and discussion

3.1. Oxyapatite formation

The formation of oxyapatite is best understood by examining some coatings produced under different spraying conditions. Since no secondary plasma gas is used in the first experiment, the changes can be attributed totally to the increased flow rate. An increase in the primary gas flow rate has little effect on the power of the plasma. The main influence is the higher particle velocity [20] which produces a higher degree of molten particle flattening upon impact with the substrate. This effect does not introduce other crystalline phases but alters the proportion of phases. A higher gas flow rate increases the amount of amorphous phases. The remaining crystalline phases of significant quantity consist of hydroxyapatite or oxyapatite. Oxyapatite is seen most clearly as the appearance of the left shoulder on the (0 0 4) peak (Fig. 3a). Both apatite phases decrease in quantity but the hydroxyapatite response appears to be more sensitive (Fig. 3c). The same tendency is observed, when cooling gas is applied to the coating during the coating operation i.e., the hydroxyapatite content decreases more rapidly compared to oxyapatite (Fig. 3b and d).

A model can be used to explain the phases within the coating (Fig. 4). The two different stages represented in the model involve firstly, the change in droplet chemistry during passage through the plasma and secondly, the formation of a lamella upon impact with the substrate. The coating is produced by the impact of successive droplets onto the already solidified lamella. The regions in the flattened particle consist of the amorphous phase, hydroxyapatite and oxyapatite.

As the particle is heated in the plasma, the outside will be heated to a higher temperature than the core, where the temperature difference is dependent upon the heat transfer within the particle [21]. Any changes in chemistry will thus occur in the shell and will progress towards the centre. The low intrinsic thermal conductivity of hydroxyapatite ($0.013\ \mathrm{Wm^{-2}K^{-1}}$) [22] minimizes chemical changes in the particle; nevertheless, the particle is unavoidably molten by the high heat transfer from the plasma. The surface of the hydroxyapatite particle becomes dehydroxylated upon being heated in the plasma, as indicated on the left-hand side of Fig. 4 labelled "Process". Dehydroxylation can commence at about 900 °C and occurs at a higher rate at greater temperatures [2, 23].

The depth of hydroxyl ion removal and the associated concentration gradient depends upon heating time and the intensity of the heat source. Particle flight of the order of milliseconds at plasma temperatures in excess of 3000 K represents a typical thermokinetic

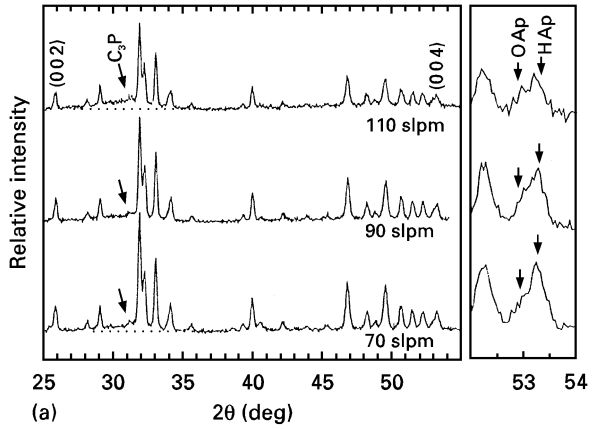

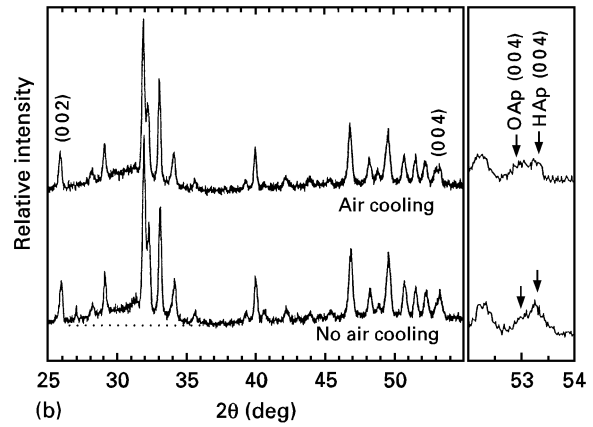

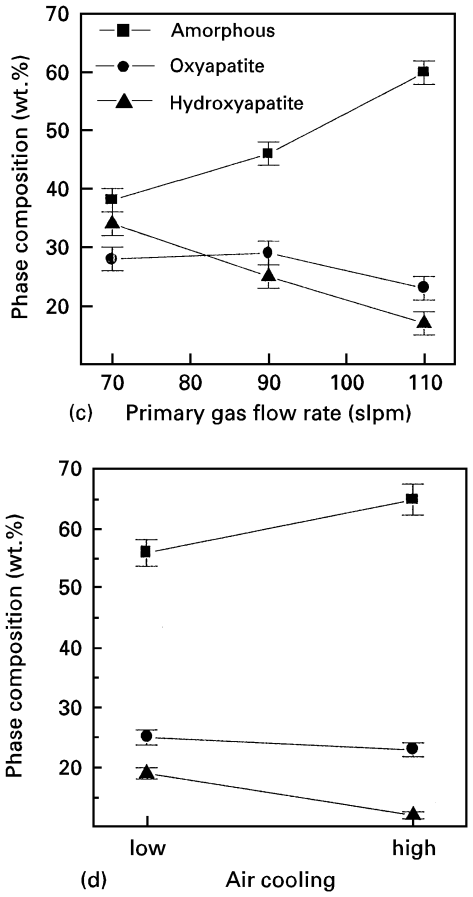

Figure 3 X-ray diffraction patterns of hydroxyapatite coatings produced at (a) increasing primary plasma gas flow rate (70, 90 and 110 standard litres per minutes (slpm) and (b) various cooling conditions. The amounts of the amorphous phase, hydroxyapatite (HAp) and oxyapatite (OAp) in the coatings calculated from (a) and (b) are shown in (c) and (d). The main tricalcium phosphate (C_3P) peak is shown in (a).

particle history in a plasma. These conditions are sufficient to produce a dehydroxylated shell. The particle size distribution in the spray powder is important, such that the extent of dehydroxylation will be different for each particle. The smaller particle will be prone to a higher level of dehydroxylation.

The composition of the inner core and the cooling conditions of the molten droplet collectively determine the phase that will form. It is assumed that the hydroxyl-deficient shell remains upon forming a lamella. As the molten particle impacts the substrate, the dehydroxylated area in contact with the substrate forms the amorphous phase [24] but the hydroxylated area is more likely to form the crystalline phase, owing to a higher driving force for crystallization. Further, from the substrate, the cooling rate is lower owing to heat dissipation through the solidified material and so the dehydroxylated portion, not participating in the amorphous phase formation, will crystallize to oxyapatite. Oxyapatite requires small atomic rearrangements to occur for crystallization and, given a fast cooling rate, will crystallize in preference to tricalcium phosphate and tetracalcium phosphate. Heterogeneous nucleation of oxyapatite on the already-formed hydroxyapatite creates a misfit of 1% which is small enough for a coherent interface [25]. A solid solution of oxyapatite and hydroxyapatite is most likely to occur at the interface and so the growth of hydroxyapatite will continue as oxyapatite in response to the depleted hydroxyl concentration at the top of the lamellae.

If the cooling conditions are sufficiently slow, hydroxyapatite and oxyapatite are produced corresponding to the hydroxyl ion concentration in the melt. At higher cooling rates the dehydroxylated region forms an amorphous phase and, at still higher cooling rates, the hydroxylated region can also form an amorphous phase. Fig. 3 is an example of a greater degree of flattening which produces higher cooling rates for the molten particles induced by a higher velocity. More of the hydroxyl-rich region is subjected to high cooling rates and subsequently forms the amorphous phase. The oxyapatite content does not change as markedly as the hydroxyapatite content owing to the position in the splat. The location on the top surface, which represents the dehydroxylated region of the splat, experiences the lowest cooling rates in the flattened particle and so a crystalline phase is most likely to form. Similarly, for the case of air cooling, the cooler substrate provides a larger thermal gradient and facilitates a higher cooling rate, producing more amorphous phase and less hydroxyapatite, and thus accentuating the detection of oxyapatite.

The deposition of successive layers will increase the temperature of the underlying coating. Air cooling provides a means of counterbalancing the effects of recalescence and the heat dissipation through the coating. This heat, otherwise, may be sufficient to produce crystallization of the amorphous phase to hydroxyapatite or oxyapatite and diffusion of hydroxyl ions to produce oxyhydroxyapatite.

In addition to process-induced effects, the powder preparation may influence the phase content of the

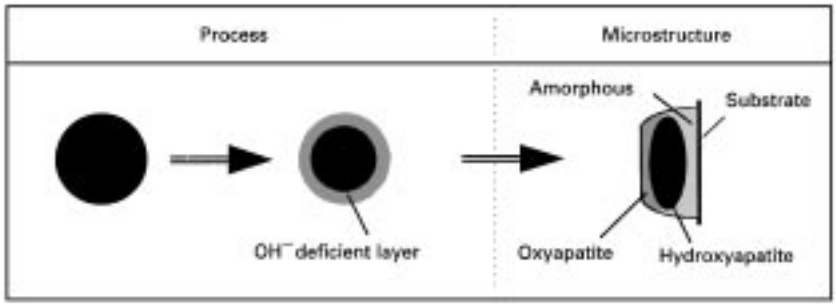

Figure 4 A schematic diagram showing the dehydroxylation of the particle during flight in the plasma and the phase regions in a single lamella. Separate regions in the flattened particle show the amorphous phase, hydroxyapatite and oxyapatite.

coating. The amount of oxyapatite can be enhanced by using a dehydroxylated powder.

3.2. Reactivity of oxyapatite

Oxyapatite is reactive and will transform to hydroxyapatite in contact with water vapour [12], to lower its free energy [26]. A coating investigated after plasma spraying shows a tendency for hydroxyl absorption and 8 wt% of oxyapatite is converted to hydroxyapatite as detected by X-ray diffraction (Fig. 5). Other phases appear to remain in the same quantity. Initially, moisture is adsorbed owing to the hydrophilic nature of the calcium phosphates [27] and then further absorbed into the structure. It cannot be discerned whether the dehydroxylated amorphous phase absorbs hydroxyl ions but the lower density of amorphous phases suggests that this might be an easier path for hydroxyl transport. The depth of OH^- absorption into the coating cannot be obtained from the X-ray diffraction pattern since the signal arises from all the coating up to a depth of about 8 μm. The absorption kinetics are mainly controlled by the partial pressure of water and the coating temperature. It must be noted that residual stresses that are created during coating manufacture [28–30] and structural imperfections [31, 32] in the oxyapatite can assist the transformation from oxyapatite to hydroxyapatite.

Conditions that could lead to the hydroxylation can occur during the spraying process or after coating manufacture. A cooling jet with compressed air that is not completely dry will supply water molecules to the surface and lead to subsequent hydroxylation before the next molten particle impinges onto the surface. Each lamellae could absorb water more easily at the elevated temperature of the coating as opposed to room- temperature conditions after the component has been sprayed. Additionally, if the coated implant is stored in humid conditions, hydroxylation can take place. Filiaggi *et al.* [33] heat treated hydroxyapatite coatings in a vacuum (less than 10^{-6} Torr) sufficient to produce a 62% dehydroxylation at the selected heat treatment temperature and observed delamination of the coating when exposed to humid conditions at room temperature. One possibility leading to delamination is lattice expansion taking place from hydroxylation of the coating to produce hydroxyapatite.

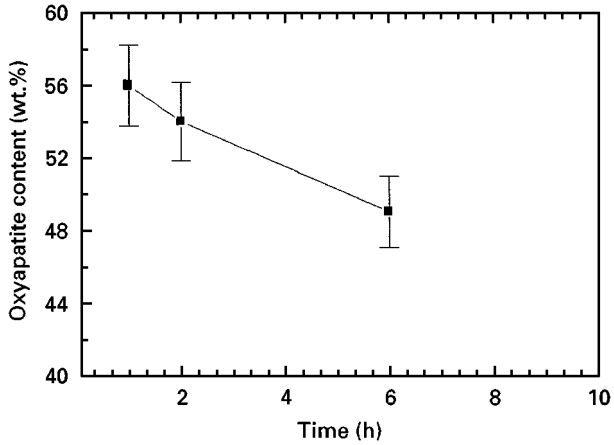

Figure 5 The change in oxyapatite content of a coating at room temperature immediately after the spraying operation.

The effects of transformation to hydroxyapatite have been observed independently by Chern Lin *et al.* [34] with the measurement of coating bond strength at different humidities. A larger decrease in bond strength was recorded at 95% humidity compared with 30% humidity at room temperature, presumably because of phase-transformation-induced cracking.

A fixed water vapour pressure is required to ensure material stability. The water vapour pressure to sustain a certain hydroxyl content within the hydroxyapatite lattice varies with temperature and becomes noticeable above 600°C, (Fig. 6). The hydroxyl (or structural water) content of hydroxyapatite can best be represented by $Ca_{10}(PO_4)_6(OH)_{2-2x}O_xV_x$ where V is a neutral vacancy in the OH^- sublattice, at equilibrium with water vapour at a specific partial pressure of p Torr. x represents the number of vacancies which are accompanied by bivalently charged oxygen ions.

The following reaction, earlier stated by Seuter [35], can be viewed as an equilibrium between hydroxide and oxygen ions under the influence of a partial water vapour pressure:

$$2OH^-\ (s) = O^{2-}\ (s) + V(s) + H_2O\ (g) \qquad (1)$$

From the law of mass action and using ΔH with a value of 251 kJ mol^{-1} [35],

$$\frac{px^2}{(2-2x)^2} = K(T) \qquad (2)$$

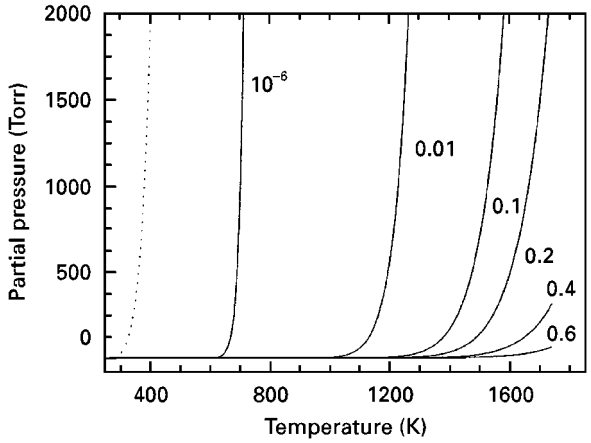

Figure 6 The partial pressure of water vapour required to sustain a certain vacancy concentration within hydroxyapatite. The figure is a graphical representation of equation (2). x represents the vacancy number which at a value of 1 denotes oxyapatite. Intermediate values represent an oxyhydroxyapatite. The dew point for water for the lower temperatures is indicated by a dotted curve.

where $K(T) = 1.2 \times 10^9 \exp(-\Delta H/RT)$. The coating analysed with synchrotron radiation revealed the same oxyapatite phase (Fig. 7a), as observed in Fig. 3 by conventional X-ray diffraction analysis. Tricalcium phosphate positioned at $Q = 2.2$ was approximately constant at less than 5 wt% and did not change with depth. An amorphous phase is also present but is difficult to observe owing to the low scattering power of the amorphous phase. The amount of amorphous phase also does not appear to change with depth.

Oxyapatite can be seen both at the (0 0 2) and (0 0 4) peak locations in using a small X-ray energy of 5.8 keV. With increasing X-ray penetration, the titanium from the substrate obscures the (0 0 4) peak of apatite. The (0 0 2) peak, however, is not masked with other peaks and can be used to analyse further changes with depth. An analysis of this peak indicated an increase in oxyapatite with depth (Fig. 7b). The subsurface response of the coating is representative of the bulk as-sprayed coating and is more representative of the high level of dehydroxylation of the molten particle before impact with the substrate. After spraying, the outside surface becomes enriched in hydroxyl content according to the vapour pressure of water in the atmosphere.

When such a coating is implanted into the body, it is expected that the initial dissolution of the surface layer will reveal an underlying coating material of a different phase composition. Initial studies have shown that oxyapatite has a higher solubility than hydroxyapatite [36]. The performance of the implant after insertion is thus dependent upon the chemical phase distribution and microstructure throughout the coating.

4. Conclusions

Plasma spraying of hydroxyapatite produces a crystalline apatite and an amorphous phase. The apatite phases present depends upon the thermal history of the particle within the plasma flame. A higher heat transfer to the traversing particle produces a greater level of dehydroxylation. This dehydroxylated melt will form an amorphous phase at those locations with a fast cooling rate and oxyapatite at lower cooling rates.

The stability of the coating prior to implantation depends upon the partial water vapour pressure. The surface of the coating will take up moisture from the atmosphere to form a hydroxylated layer. X-ray diffraction with synchrotron radiation has found that the oxyapatite content of a coating increases with increasing depth. This will have an effect on the properties of the coating when implanted into the body and might undergo further change after immersion in physiological fluids.

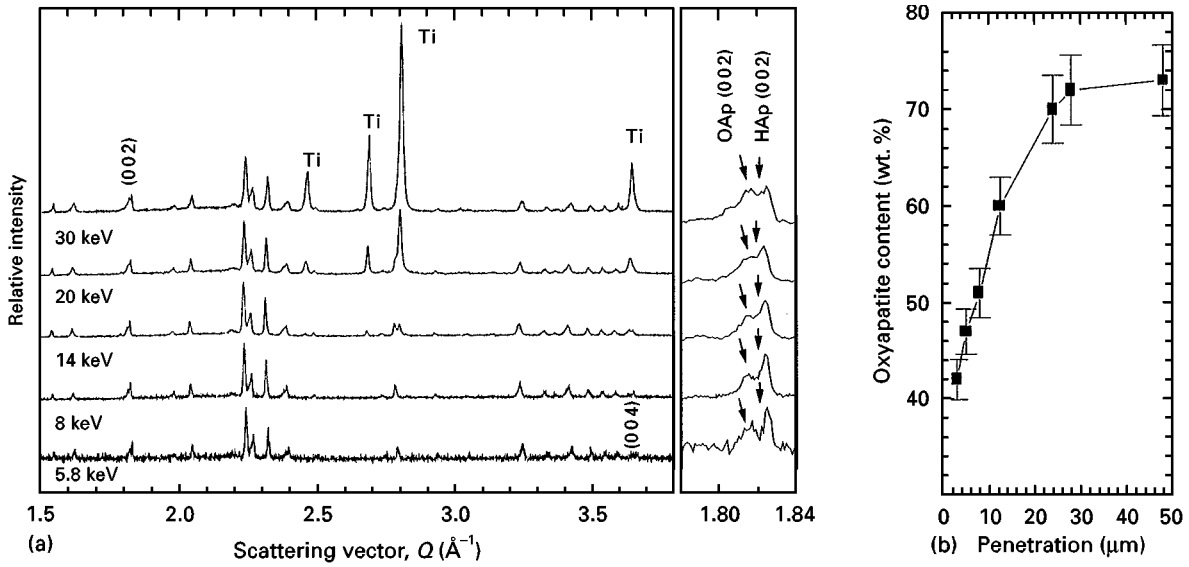

Figure 7 Detection of oxyapatite in (a) X-ray diffraction patterns and (b) the amount of oxyapatite in proportion to both apatites (hydroxyapatite and oxyapatite) as a function of coating depth. The inset of (a) shows a magnification of the (0 0 2) peak of oxyapatite and hydroxyapatite.

Acknowledgements

Research was carried out in part at the National Synchrotron Light Source at Brookhaven National Laboratory, which is supported by the U.S. Department of Energy, Division of Materials Sciences and Division of Chemical Sciences. The SUNY X3 beamline at NSLS is supported by the Division of Basic Energy Sciences of the U.S. Department of Energy under grant DE-FG02-86ER45231.

References

1. T. NEGAS and R. S. ROTH, *J. Res. Natl. Bur. Stand. A* **72** (1968) 783.
2. P. V. RIBOUD, *Ann. Chim.* **8** (1973) 381.
3. H. OWADA, K. YAMASHITA, T. UMEGAKI, T. KANAZAWA and M. NAGAI, *Solid State Ionics* **35** (1989) 401.
4. M. NAGAI, T. NISHINO and T. SAEKI, *Sens. Actuators* **15** (1988) 145.
5. K. YAMASHITA, H. OWADA, T. UMEGAKI, T. KANAZAWA, and K. KATAYAMA, *Solid State Ionics* **40–41** (1990) 918.
6. S. RADIN and P. DUCHEYNE, in "Characterization and performance of calcium phosphate coatings for implants", ASTM Special Technical Publication 1196 (American Society for Testing and Materials, Philadelphia, PA, 1994), p. 111.
7. H. DASARATHY, C. RILEY and H. D. COBLE, *J. Biomed. Mater. Res.* **27** (1993) 477.
8. R. C. TACKER and K. A. GROSS, *Biomaterials* (1998) submitted.
9. R. McPHERSON, N. GANE and T. J. BASTOW, *J. Mater. Sci., Mater. Med.* **6** (1995) 327.
10. K. A. GROSS, V. GROSS and C. C. BERNDT, *J. Amer. Ceram. Soc.* **81** (1998) 106.
11. J. C. TROMBE, *Ann. Chim.* (*Paris*), *14th Ser.* **8** (1973) 335.
12. G. MONTEL, G. BONEL, J. C. TROMBE, J. C. HEUGHEBAERT and C. REY, *Pure Appl. Chem.* **52** (1980) 973.
13. D. M. LIU, H. M. CHOU and J. D. WU, *J. Mater. Sci., Mater. Med.* **5** (1994) 147.
14. K. A. GROSS and C. C. BERNDT, *J. Biomed. Mater. Res.* **39** (1998) 580.
15. B. AUMÜLLER, A. N. KIRKBRIDE, R. ZELLER and H. W. BERGMANN, *Materialwissenschaft Werkstofftechn.* **27** (1996) 72.
16. C. Y. YANG, B. C. WANG, E. CHANG and J. D. WU, *J. Mater. Sci., Mater. Med.* **6** (1995) 249.
17. L. G. ELLIES, D. G. A. NELSON and J. D. B. FEATHERSTONE, *Biomaterials* **13** (1992) 313.
18. B. D. CULLITY, "Elements of X-ray diffraction" (Addison-Wesley, Reading, MA, 1978).
19. P. PREDECKI, *Powder Diffraction* **8** (1993) 122.
20. P. FAUCHIAS, J. F. COUDERT, M. VARDELLE, A. VARDELLE and A. DENOIRJEAN, *J. Thermal Spray Technol.* **1** (1992) 117.
21. M. VARDELLE, A. VARDELLE, A. DENOIRJEAN and P. FAUCHAIS, *Mater. Res. Soc. Proc.* **190** (1991) 175.
22. T. KIJIMA and M. TSUTSUMI, *J. Amer. Ceram. Soc.* **62** (1979) 455.
23. R. M. H. VERBEECK, H. J. M. HEILIGERS, F. C. M. DRIESSENS and H. G. SCHAEKEN, *Z. Anorg. Allg. Chem.* **466** (1980) 76.
24. K. A. GROSS, C. C. BERNDT and H. HERMAN, *J. Biomed. Mater. Res.* **39** (1998) 407.
25. D. A. PORTER and K. E. EASTERLING, in "Phase transformations in metals and alloys", (Chapman and Hall, London, 1990) p.158.
26. E. J. DUFF, *J. Inorg. Nucl. Chem.* **34** (1972) 853.
27. R. Z. LE GEROS, G. BONEL and R. LEGROS, *Calcif. Tiss. Res.* **26** (1978) 111.
28. S. TADANO, M. TODOH, J.-I. SHIBANO and T. UKAI, *Jpn. Soc. Mech. Engng Int. J.* **40** (1997) 328.
29. J. C. KNOWLES, K. A. GROSS, C. C. BERNDT and W. BONFIELD, *Biomaterials* **17** (1996) 639.
30. S. R. BROWN, I. G. TURNER, H. REITER, *J. Mater. Sci., Mater. Med.* **5** (1994) 756.
31. L. C. LOVELL, *Acta Metall.* **6** (1958) 775.
32. G. DACULSI, R. Z. LE GEROS, J. P. LE GEROS and D. MITRE, *J. Appl. Biomater.* **2** (1991) 147.
33. M. J. FILIAGGI, R. M. PILLIAR and N. A. COOMBS, *J. Biomed. Mater. Res.* **27** (1993) 191.
34. J. H. CHERN LIN, M. L. LIU and C. P. JU, *Dent. Mater.* **9** (1993) 286.
35. A. M. J. H. SEUTER, in "Reactivity of Solids" (Chapman & Hall, London, 1972) p. 806.
36. K. A. GROSS, PhD dissertation, State University of New York at Stony Brook (1995).

Received 9 January 1997
and accepted 11 May 1998